Spatio-temporal dynamics of sediment transfer systems in landslide-prone alpine catchments

François Clapuyt[1], Veerle Vanacker[1], Marcus Christl[2], Kristof Van Oost[1], Fritz Schlunegger[3]

[1] Earth and Life Institute, Georges Lemaître Centre for Earth and Climate Research, Université Catholique de Louvain, Place Pasteur, 3 Bte L4.03.08, 1348 Louvain-la-Neuve, Belgium.

[2] Laboratory of Ion Beam Physics, ETH Zurich, Otto-Stern-Weg 5, 8093 Zürich, Switzerland.

[3] Institut für Geologie, Universität Bern, Institut für Geologie, Baltzerstrasse 1+3, 3012 Bern, Switzerland.

Correspondence to: François Clapuyt (francois.clapuyt@uclouvain.be).

Abstract. Tectonic and geomorphic processes drive landscape evolution over different spatial and temporal scales. In mountainous environments, river incision sets the pace of landscape evolution, and hillslopes respond to channel incision by e.g. gully retreat, bank erosion and landslides. Sediment produced during stochastic landslide events leads to mobilisation of soil and regolith on the slopes that can later be transported by gravity and water to the river network during phases of hillslope-channel geomorphic coupling. The mechanisms and scales of sediment connectivity mitigate the propagation of sediment pulses throughout the landscape and eventually drive the contribution of landslides to the overall sediment budget of mountainous catchments. However, to constrain the timing of the sediment cascade, the inherent stochastic nature of sediment and transport through landsliding requires an integrated approach accounting for different space and time scales. In this paper, we examine the sediment production on hillslopes and evacuation to the river network of one landslide, i.e. the Schimbrig earthflow, affecting the Entle river catchment located in the foothills of the Central Swiss Alps. We quantified sediment fluxes over annual, decadal and millennial time scales using respectively UAV-SfM techniques, classic photogrammetry and in-situ produced cosmogenic radionuclides. At the decadal scale, sediment fluxes quantified for the period 1962-1998 are highly variable and are not directly linked to the intensity of sediment redistribution on the hillslope. At the millennial scale, landslide occurrence perturbs the regional positive linear relationship between sediment fluxes and downstream distance as the landslide-affected Schimbrig catchment is characterised by a decrease in sediment fluxes and a strong variability. Importantly, the average decadal sediment flux of the Schimbrig catchment is two orders of magnitude higher than millennial sediment fluxes computed over the same spatial extent. The discrepancy between decadal and millennial sediment fluxes, combined to the highly variable annual sediment evacuation from the hillslopes to the channel network suggest that phases of hillslope-channel geomorphic coupling are short and intermittent. During most of the time, the first-order catchments are transport-limited and sediment dynamics in the headwaters are uncoupled from the fluvial systems. In addition, our unique spatio-temporal database of sediment fluxes highlights the transient character of the intense geomorphic activity of the Schimbrig catchment in a regional context. Its decadal sediment flux is of the same order of magnitude than the background sediment flux going out of the entire Entle river catchment. Over the last 50 years, the Schimbrig catchment, which represents ca. 1% of the entire study area, provides 65 % of the sediments that the entire Entle catchment will supply over the millennial scale. These results suggest that episodic supply of sediment from landslides during intermittent phases of hillslope-channel geomorphic coupling are averaged out when considering sediment fluxes at longer time scales and larger spatial scales.

1 Introduction

The segmentation of the sediment pathway into distinct cascades is a widely used concept to describe the routing of sediment particles from sources to sinks throughout a landscape (Walling, 1983). Among other factors, e.g. topography, lithology, climate or tectonic activity (e.g. Aalto et al., 2006; Montgomery and Brandon, 2002; Whipple and Tucker, 1999), the geomorphic coupling and sediment connectivity control the efficiency of sediment transfer in geomorphic systems, and

condition the pace at which landscapes evolve through time (Bracken et al., 2015; Fryirs, 2013; Harvey, 2001; Heckmann and Schwanghart, 2013). The *geomorphic coupling* between distinct landscape elements is commonly seen as a measure of how individual landforms are linked through sediment transport (e.g. Harvey, 2001; Heckmann and Schwanghart, 2013), while the term *sediment connectivity* has been employed for characterizing the transfer of sediments at a larger scale which includes

5 potential sources and sinks within a geomorphic system (Bracken et al., 2015). Accordingly, a large connectivity requires an implicit geomorphic coupling between distinct landscape units (Bracken et al., 2015).

In this context, most research has focused on how the connectivity between landslides and trunk channels influences the overall sediment budget of a landscape. Because landslides are a dominant source of sediments in mountainous environments (Korup et al., 2010; Vanacker et al., 2003), one can expect that the magnitude and frequency of landsliding (e.g. Crozier and Glade,

10 1999; Hovius et al., 1997; Malamud et al., 2004) will directly impact the bulk sediment flux of a drainage basin. Nevertheless, the contribution of landslides to the overall sediment budget is still poorly constrained: landslides stochastically supply sediment to the river network, and their geomorphic efficiency varies according to the mechanisms and scales of sediment connectivity (Benda and Dunne, 1997; Bennett et al., 2014). Field studies have shown that the landscape capacity to buffer sediment fluxes from landslides can vary from several years (Berger et al., 2011; Fuller and Marden, 2010) to decades (e.g.

15 Bennett et al., 2013; Schwab et al., 2008) and millennia (e.g. Wang et al., 2017). The inherent stochastic nature of sediment production and transport through landsliding prohibits linear upscaling of small-to-medium scale geomorphic process assessments, as well as extraction of a particular erosion mechanism from the entire sediment cascade using long-term/large-scale methods (Bennett et al., 2014; Bracken et al., 2015).

Although the analysis of spatio-temporal patterns of the sediment cascade can provide insights in sediment transfer

20 mechanisms in landslide-affected catchments, few studies attempted to integrate different spatial and temporal scales to assess landscape response to landslide sediment supply and transport. Mackey et al. (2009) compared surface displacement velocities of an earthflow derived from historical airphotos with sediment transport rates derived from meteoric [10]Be inventories. Their study showed that the displacement rate of the Eel earthflow (northern California) was highly episodic in time, as the earthflow acted as a source of sediments over the last 150 years with an erosion rate that was more than 20 times faster than the millennial

25 sediment transport rate. In a similar study, Delong et al. (2012) measured surface displacement rates of the Mill Gulch earthflow from light detection and ranging (LiDAR) data and compared this data with [10]Be-derived denudation rates of two adjacent catchments. These authors reported short-term denudation rates (2003 and 2007) that were similar to long-term ones. These two case studies show the assets of a spatio-temporal approach for unravelling the mechanisms of sediment connectivity in landslide-prone environments.

30 In this study, we examined the propagation of sediment pulses in landslide-prone environments, from sediment production at the hillslopes to sediment transport and delivery to the river network. By integrating geomorphic assessments at different spatio-temporal scales, and utilizing information on the propagation of sediment pulses along the sediment cascade, we

considered the evacuation of landslide-derived sediment to the colluvial and fluvial domains. Sediment fluxes were assessed over annual, decadal and millennial time scales using respectively UAV-SfM techniques, classic photogrammetry and in-situ produced cosmogenic radionuclides. In this study, we posit that sediment fluxes in landslide-prone alpine catchments can be highly variable in space and time, with long periods of quiescence during which sediment is temporarily stored on the hillslopes and short episodes of high sediment flux when hillslopes and channel are coupled through superimposed debris flows.

2 Conceptual framework

Within the sediment cascade, landslides stochastically act as a major sediment source on hillslopes. Here, we propose a conceptual framework (Figure 1) that may facilitate the quantification of spatio-temporal patterns of sediment cascades in landslide-prone catchments. Landslides can mobilise soil and regolith material (Figure 1a) that can temporarily accumulate on the slopes (Figure 1b), and become available for further mobilisation and transport downslope. In decoupled hillslope-channel systems, sediments remain on hillslopes as landslide colluvial fans before being gradually depleted and transported to the river network by rainfall-induced and stochastic superimposed debris flows (e.g. Benda and Dunne, 1997b; Schwab et al., 2008). Therefore, the stochastic behaviour of sediment supply on the slopes and sediment transport in the river network gives the landscape a certain capacity to buffer sediment transfer within the sediment cascade (Gran and Czuba, 2017). The temporal scale of the buffering capacity can be highly variable, and vary from a number of years (e.g. Berger et al., 2011; Fuller and Marden, 2010; Sutherland et al., 2002), to decades (e.g. Bennett et al., 2013; Schwab et al., 2008), and millennia (e.g. Dingle et al., 2018; Wang et al., 2017; West et al., 2014). In configurations where hillslopes are physically linked to channels (Figure 1c), the material derived from landsliding is effectively evacuated by the fluvial system (e.g. Berger et al., 2011; Sutherland et al., 2002; Wang et al., 2017). The hillslope-channel geomorphic coupling controls the propagation of sediment pulses from landslides to the river network (Figure 1d). In catchments with strong hillslope-channel geomorphic coupling by e.g. debris flows entering the channel reach, we might expect to see rapid response of the fluvial system to geomorphic events, such as stochastic landslide events. In well-coupled systems, the landslide-derived sediment fluxes for the hillslopes should show good correspondence with the catchment-wide sediment flux.
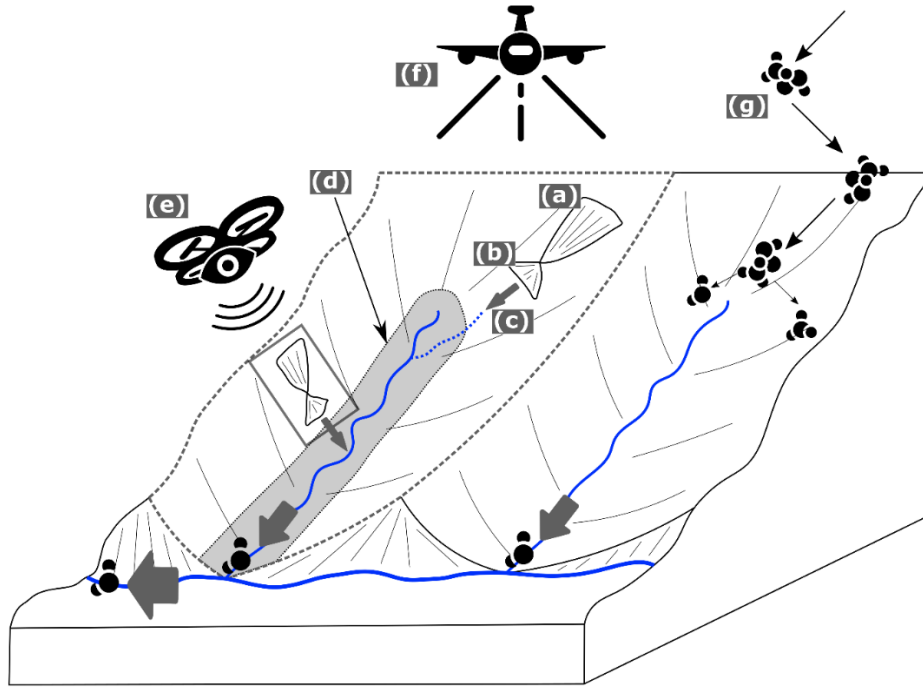
Figure 1: Conceptual framework of the sediment dynamics in alpine landslide-affected first-order catchments. (a) Landslides are a stochastic process that mobilise soil and regolith downslope. (b) Landslide-derived material can temporarily be stored on the slopes in landslide colluvial fans, (c) and/or be evacuated by debris flows to the fluvial system. (d) Hillslope-channel geomorphic coupling (by e.g. slope failures induced by river undercutting) is particularly important for understanding the response of the geomorphic system to sediment pulses. The quantification of sediment fluxes is achieved using (e) UAV-SfM framework, (f) classic photogrammetry and (g) in-situ produced cosmogenic radionuclides.

The downslope propagation of sediment from the hillslopes sources, namely landslides, debris flows and colluvial fans, to the channel network can be constrained using a time-space approach. In this conceptual framework, we propose to combine information derived from UAV-SfM techniques, classic photogrammetry and in-situ produced cosmogenic radionuclides to quantify spatio-temporal patterns in denudation rates and sediment fluxes. Catchment-scale denudation rates quantify the surface lowering per unit of time ($L\ T^{-1}$) and are scale-invariant. Sediment fluxes record the volume of sediment exported or evacuated from a given surface area per unit of time ($L^3\ T^{-1}$), and quantify the rate of sediment transfer between landscape units, i.e. between hillslopes and channels. At annual scale, the geomorphic processes in the hillslope domain (10^0-10^1 km^2) can be monitored using very high-resolution topographic reconstructions (Figure 1e). At the decadal scale, the sediment dynamics of first-order catchments can be quantified from time-series of digital elevation models using classic photogrammetry (Figure 1f). Catchment-averaged cosmogenic radionuclide (CRN)-derived denudation rates provide integrated geomorphic process rates over the millennial time scale (Figure 1g). In the discussion of the results of this study, we will refer to this conceptual framework (Figure 1) to contextualise the results.

3 Material and methods

3.1 The Entle and Schimbrig catchments

Our study area is located in the northern foothills of the Central Swiss Alps, between Bern and Lucerne (Figure 2). The Entle catchment has a drainage basin of 64 km^2, with an elevation ranging between 680 m a.s.l. at the outlet near Entlebuch village and 1,815 m on the Schimbrig summit. The study area lies on the intersection between the Swiss Plateau, i.e. the Molasse Basin, and the frontal thrusts of the Alpine orogeny. The Molasse unit, covering the lower reaches of the catchment, is composed of Late Oligocene conglomerate bedrock knobs, forming erosion-resistant low ridges. The intermediate part of the catchment is covered by the Subalpine Flysch, while the higher SW-NE-oriented ridge is composed of Cretaceous carbonate rocks of the Helvetic thrust sheet (Schlunegger et al., 2016a; Figure 2). The Entle catchment is dissected by a 7 km-long central inner gorge with two tributaries, i.e. the Grosse and the Kleine Entle, that are deeply incised into a more than 100 m thick unconsolidated glacial till. The glacial till was deposited during repetitive and extensive glaciations during the Pleistocene. Lateral and terminal moraines deposited by the Entle glacier during the Last Glacial Maximum (LGM) are dissected by the Grosse and Kleine Entle rivers up to the headwaters (Figure 2). The inner gorge contains knickzones in its longitudinal profile, and several cut terraces are visible. A ^{10}Be-based sediment budget, which covers the last ca. 2,000 years, highlighted that incision rates in the inner gorge are more than 4 times higher than in the non-incised reaches (Van den Berg et al., 2012). The study area experiences three types of mass movement processes over distinctive landscape units. Landslides categorised as earthflows mainly affect the flysch areas. This type of mass movement is very common in flysch sedimentary sequences, and represents more than 30% of all mass movements in Switzerland according to Lateltin et al (1997). Near the summits, rock falls are common phenomena; and the sidewalls of river valleys are subject to widespread rotational and translational landslides.
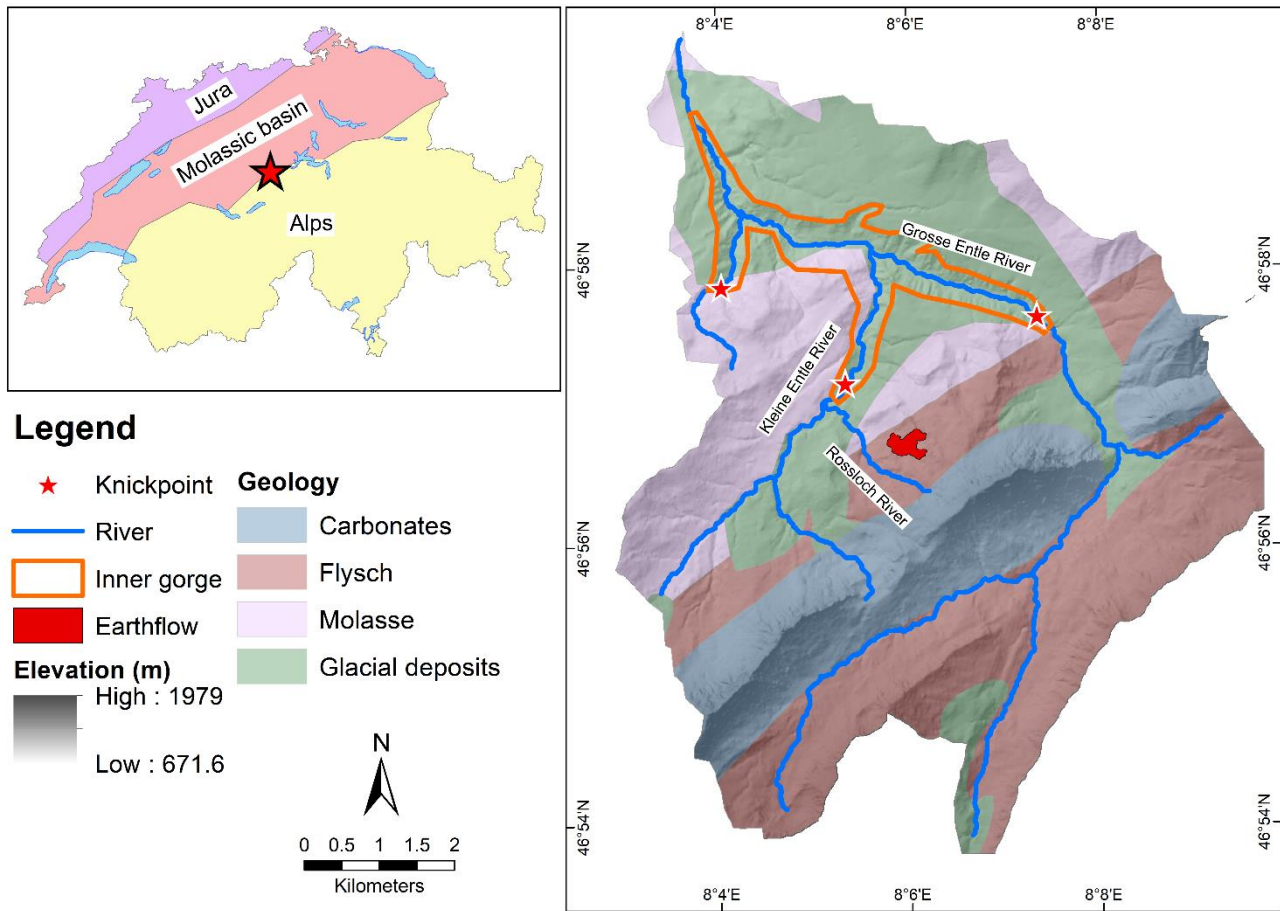
Figure 2: Simplified geological and geomorphological settings of the Entle river catchment (after Van den Berg et al., 2012; Schlunegger et al., 2016b). Inset: Location of the study area in Switzerland.

Within the Entle river catchment, an earthflow named Schimbrig has been particularly active over the last 150 years, acting as a sediment factory by excavating and mobilising sediments because of its deep rotational structure (Clapuyt et al., 2017; Lopez-Saez et al., 2017; Savi et al., 2013; Schwab et al., 2008). It is located in the first-order Schimbrig catchment, the latter draining successively into the Rossloch river and the Kleine Entle, before entering the trunk river, i.e. the Grosse Entle. The earthflow occurs on the hillslopes of the Schimbrig ridge and is not directly connected to the Schimbrig stream, except during short episodes when superimposed debris flows occur (Schwab et al., 2008). The Schimbrig earthflow consists of a fine-grained matrix of silt and mud, with centimetric to decimetric large clasts (Clapuyt et al., 2017). The internal structure of the earthflow is complex with nested rotational units (Clapuyt et al., 2017). Field observations revealed that a major earth slide with an up-to 12 m surface lowering occurred in the summer of 1994 after a succession of heavy precipitation events, followed by debris flows until March 1995 (Schwab et al., 2008). The intensity and spatial pattern of sediment redistribution, as well as the internal

structure of the earthflow have rapidly evolved at the annual and decadal scale (Clapuyt et al., 2017; Schwab et al., 2008). The Schimbrig catchment also experiences scree slopes-like erosion processes in the upper part on the Schimbrig ridge. Eroded material is stored at foot of slope, above river sources. Within the Schimbrig catchment, the described earthflow affects ca. 25% of the area and is the only active process in the catchment.

3.2 Annual sediment fluxes

The annual sediment fluxes of the active part of the Schimbrig earthflow (Figure 3) were derived from time series of very high-resolution topographic datasets from Clapuyt et al. (2017). The earthflow has a rotational structure, and is the dominant source of sediment on the hillslopes. By quantitatively comparing topographic datasets, we assessed spatial patterns of surface *lowering*, i.e. a decrease in ground elevation, and *bulging*, i.e. an increase in ground elevation. The overall sediment budget of the area affected by the earthflow, i.e. the difference between surface lowering and bulging, is indicative of the change in sediment volume through time. The sediment flux is derived at the base of the hillslopes at the transition between the hillslope and fluvial domains, and represent the net flux of sediment from the earthflow to the Schimbrig river. The earthflow acts as a pure sediment source on the hillslope.
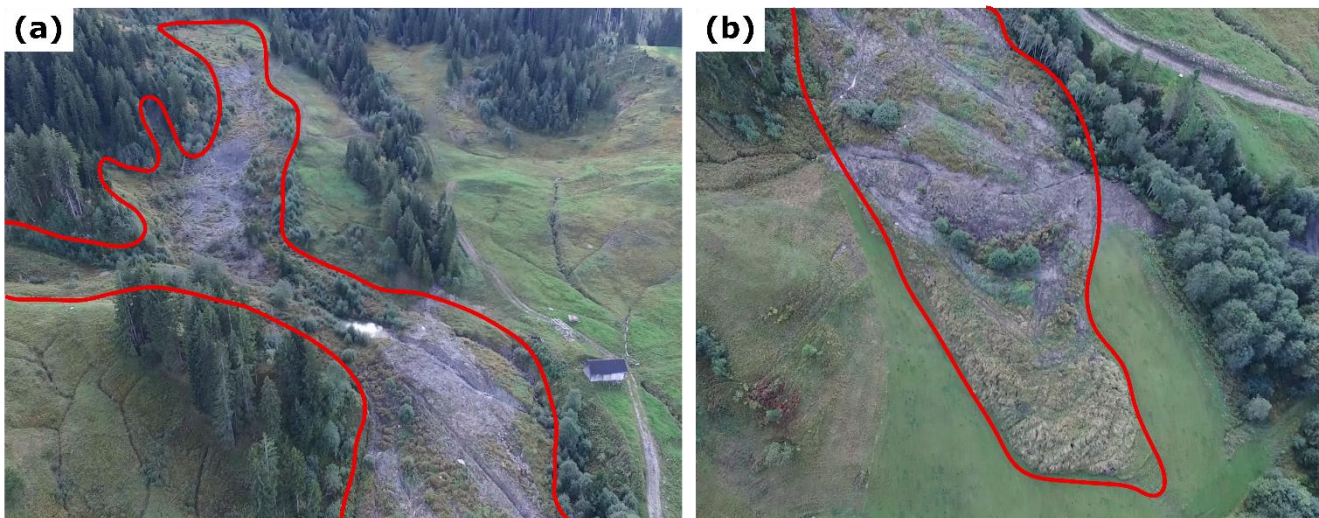
Figure 3: Illustration of the Schimbrig earthflow acting as a source of sediment in the river catchment. (a) Upper part with surface subsidence. (b) Toe of the earthflow with surface bulging.

The 3D topographic reconstructions were computed using the structure-from-motion algorithm (SfM) based on aerial photographs acquired by an unmanned aerial vehicle (UAV). Point clouds were subsequently interpolated into digital surface models (DSM) at a spatial resolution of 0.04 m, defined based on the density of the point clouds. The accuracy of the time series is ranging between 0.20 m and 0.24 m. Acquisition dates are October 2013, June 2014 and October 2015. As part of this

sediment flux assessment, only the dataset of the 2014-2015 time interval was used because it covers the full spatial domain of the Schimbrig earthflow. The sediment budget was quantified from a digital elevation model of differences (DoD) between DSMs, using the Geomorphic Change Detection software (Wheaton et al., 2010). In this paper, values are eventually reported on an annual basis instead of over the entire period of interest (as in Clapuyt et al., 2017). Detailed information about the

5   methodology and extended results are available in Clapuyt et al. (2017). Errors reported at the annual scale were computed based on a uniform limit-of-detection applied on each topographic surface. Therefore, the associated error to the annual sediment fluxes should be seen as a maximum value. It is likely that spatializing the error on very high-resolution topographic measurements, i.e. accounting for the spatial variation of photogrammetric and georeferencing precisions of the reconstructions, would lead to an increase of the signal-to-noise ratio as shown by James et al (2017).

10   **3.3 Decadal sediment fluxes**

The sediment fluxes at decadal scale were derived from Schwab et al. (2008), who assessed sediment transport by the Schimbrig earthflow and associated slopes, i.e. the *Schimbrig catchment* (Figure 4), and linked it with suspended sediment loads from a gauging station in the trunk stream, i.e. the *Waldemme river*. The authors based their analysis on a time series of DEMs derived from classic photogrammetry of aerial photographs acquired in 1962, 1986, 1993 and 1998. Each image of

15   stereo-pairs was scanned with a ground resolution of 0.4 m and georeferenced using a differential GPS. Because of the scarcity of well-recognizable features through time, the associated volumetric errors of the photogrammetric workflow ranged between 2% for the 1986-1993 time interval and 29% for the 1962-1986 time interval. The sediment budget based on DEMs provides two metrics. The total sediment displaced corresponds to surface lowering while the total sediment exported per year, i.e. the sediment flux entering the Rossloch river, is the balance between surface lowering and bulging. The ratio between both metrics

20   indicates the percentage of sediment mass evacuated compared to the displaced mass. For this study, we converted the average sediment fluxes that were expressed in tons per year into cubic metre per year, using a material density of 2.70 g cm^{-3} following a study by Gong (2005) on similar flysch units in Switzerland. Detailed methodology and results are available in the original paper of Schwab et al. (2008).

3.4 Millennial sediment fluxes

25   The geomorphic process rates at millennial scale were assessed from catchment-averaged denudation rates derived from in-situ produced cosmogenic radionuclides in fluvial sediments. In order to get a comprehensive dataset on the spatial variation in denudation rates in the Entle catchment, we collected river sand on eight locations in and around the Schimbrig catchment (Figure 4) and combined the resulting dataset with earlier work by Van den Berg et al. (2010). The new samples were processed following the protocol described in Vanacker et al. (2007), which is similar to the one followed by Van den Berg et al. (2010).

30   After washing and sieving samples to the 0.25-1.00 mm fraction size, grains were separated using a Frantz Isodynamic Magnetic Separator. The remaining non-magnetic fraction was leached up to 10 times with 10% hydrochloric acid to remove

organic, calcium and carbonate components. Then, samples were treated up to four times with 5% hydrofluoric acid in order to dissolve anything but quartz and also remove any meteoric [10]Be left. After the leaching step, 157.8 µg of [9]Be carrier was added to the clean quartz samples containing ca. 25 g of material. The purified quartz, i.e. ca. 10% of the original sample weight, was subsequently dissolved in concentrated HF, from which beryllium was stepwise extracted using anion/cation exchange column chemistry. Remaining precipitates were oxidized and pressed into copper targets. Finally, [10]Be/[9]Be ratios were quantified using the 500 kV Tandy facility at ETH Zürich (Christl et al., 2013). These values were normalized with the in-house standard S2007N and corrected with a blank [10]Be/[9]Be ratio of $4.06 \pm 0.23 \times 10^{-15}$. Catchment-wide denudation rates were then computed from the in-situ produced [10]Be concentrations, i.e. from this study and from earlier data published by Van den Berg et al. (2010), using the catchment-averaged denudation rates from cosmogenic nuclide (CAIRN) method (Mudd et al., 2016). This open source calculator uses the topography to weight the [10]Be production rate and shielding. A 1 m digital terrain model (DTM) resampled to 30 m resolution was used to compute topographic shielding. Snow shielding was averaged for each catchment individually. Snow cover is estimated using an elevation-dependent mean annual snow cover database for Switzerland (Auer, 2003). Following Jonas et al. (2009), an empirical relationship is used to derive the snow water equivalent thickness (SWE, g cm^{-2}).We kept the default parameters from Mudd et al. (2016) to run the CAIRN model, including the sea-level high-latitude production rate of 4.30 at g^{-1} yr^{-1} (based on Braucher et al., 2011). Long-term denudation rates obtained by the CAIRN calculator were converted into sediment fluxes (m^3 yr^{-1}), by multiplying them with the catchment area.

4 Results

4.1 Schimbrig earthflow sediment dynamics at the annual scale

When focusing on the active part of the Schimbrig earthflow (Figure 4), we obtained a net mass flux of $1,000 \pm 4,000$ m^3 yr^{-1} for the 2014-2015 period (Table 1; Clapuyt et al., 2017). Accounting for the associated error, the sediment flux is considered to be null. The sediment budget for the 2013-2014 time interval supports this finding. In the eroding sites, the average denudation was 0.8 ± 0.2 m yr^{-1}, and equivalent to the accumulation that was observed in the bulging areas (Table 1). For the Schimbrig earthflow, Clapuyt et al. (2017) reported a mean horizontal displacement of ca. 6.30 m yr^{-1} in the downslope direction. The UAV-SfM derived data suggest that the earthflow has been in a dynamic equilibrium over the 2014-2015 period, with earthflow-derived material being temporarily stored on the slopes during the period of interest.

Notwithstanding the state of dynamic equilibrium, the data suggest large internal movements with a complex pattern of sediment redistribution along the slope (Clapuyt et al., 2017). A succession of areas with terrain lowering and bulging characterised the earthflow along its longitudinal axis. The earthflow was re-adjusting to a new state of equilibrium after a massive failure that occurred in 1994. The sediment redistribution on the slopes was not associated with an increased sediment export downstream. Between 2013 and 2015, the hillslope domain was disconnected from the fluvial domain.

Table 1: Sediment fluxes for the 2014-2015 time interval from the Schimbrig earthflow (Modified from Clapuyt et al. (2017), to provide sediment fluxes reported on an annual basis).

	Estimate	Error (±)
Total area of surface bulging (m^2)	10763	-
Total area of surface lowering (m^2)	9730	-
Average rate of surface bulging (m yr^{-1})	0.8	0.2
Average rate of surface lowering (m yr^{-1})	0.8	0.2
Average net depth of difference (m yr^{-1})	0.05	0.15
Sediment flux (m^3 yr^{-1})	1,000	4,000

4.2 Sediment budget of the Schimbrig catchment at decadal scale

Sediment fluxes were computed from 1962 to 1998 over the first-order catchment affected by the earthflow, down to the confluence with the Rossloch river (Table 2; Figure 4; Schwab et al., 2008). The average sediment flux per year, evacuated from the catchment, is varying over time, from $14,000 \pm 4,000$ m^3 yr^{-1} for the 1962-1986 period, to 850 ± 20 m^3 yr^{-1} for 1986-1993 to $24,000 \pm 4,000$ m^3 yr^{-1} for the 1993-1998 time interval. The data from Schwab et al. (2008) indicate that there is no clear link between the sediment fluxes exported from the Schimbrig catchment and the earthflow dynamics on the hillslopes. This is evident from the fact that the proportion of the mass evacuated from the study area to the total displaced mass varies largely between 6% and 89% (Table 2).

Table 2: Sediment fluxes between 1962 and 1998 (after Schwab et al., 2008).

Time interval	Total sediment displaced (10^3 t)	Total sediment exported (10^3 t)	Average sediment flux evacuated (m^3 yr^{-1})	Error on sediment flux (m^3 yr^{-1})	Percentage of mass evacuated compared to the displaced mass (%)
1962-1986	1,003	892	14,000	4,000	89
1986-1993	272	16	850	20	6
1993-1998	946	322	24,000	4,000	34
1962-1998	1,581	1,229	13,000	2,000	78

During the 1962-1986 period, about 89% of the displaced mass was evacuated from the catchment, suggesting that sediment storage during this period was not significant. In contrast, during the following periods (1986-1993, 1993-1998) when the major earthflow event occurred in 1994, only up to 34% of the mobilised earthflow material was evacuated.

4.3 CRN concentrations in the Entle catchment

The [10]Be concentrations reported in this study are spatially and quantitatively consistent with earlier measurements by Norton et al (2008) and Van den Berg et al. (2010) (Figure 4). Overall, the [10]Be concentrations (Table 3; Figure 4; Van den Berg et al., 2010) range from $0.15 \pm 0.53 \times 10^3$ at g^{-1} in the upper part of the Schimbrig earthflow (*CH-ENT-3*) to $5.28 \pm 0.26 \times 10^3$ at

g[-1] in the upper part of the Entle catchment, i.e. the Rothbach river (*E-9*). As the ^{10}Be concentrations of the earthflow-affected area are low, relatively high errors are reported for the ^{10}Be concentrations of the earthflow-derived sediment (Table 3). The errors subsequently propagated on the denudation rates, particularly for the samples from the Schimbrig stream draining the earthflow, i.e. *CH-ENT-1*, *CH-ENT-5* and *CH-ENT-8*.

5 **Table 3: ^{10}Be concentrations (at g^{-1}), CRN-derived denudation rates (mm kyr^{-1}) and sediment fluxes (m^3 yr^{-1}) for the Schimbrig catchment and other first-order rivers, i.e. samples CH-ENT-*, from this study and re-computed denudation rates and sediment fluxes for the Entle river catchment, i.e. samples Ent* and E-*, from Van den Berg et al. (2010).**

Sample	Drainage area (km²)	Altitude (m)	Latitude (dd)	Longitude (dd)	Measured ^{10}Be/^{9}Be ratio (×10^{-14})	^{10}Be concentration (×10³ at g^{-1})	Production scaling	Topographic shielding	Snow shielding	Denudation rate (mm ky^{-1})	Sediment flux (m³ yr^{-1})	Apparent age (yr)
CH-ENT-1	0.20	1451	46.945	8.098	1.85	0.62 ± 0.45	3.306	0.954	0.904	1000 ± 2000	300 ± 400	650
CH-ENT-2	1.96	1264	46.951	8.086	7.52	2.94 ± 0.28	2.965	0.974	0.917	260 ± 60	500 ± 100	2500
CH-ENT-3	0.16	1500	46.943	8.104	1.17	0.15 ± 0.53	3.427	0.937	0.900	5000 ± 1000	900 ± 200	130
CH-ENT-5	0.35	1373	46.946	8.097	3.50	2.32 ± 0.58	3.208	0.961	0.909	300 ± 100	120 ± 40	2167
CH-ENT-6	3.25	1306	46.942	8.077	10.03	4.12 ± 0.28	3.069	0.950	0.914	180 ± 40	600 ± 100	3611
CH-ENT-7	4.54	1336	46.942	8.076	6.88	2.57 ± 0.27	3.112	0.960	0.912	300 ± 70	1400 ± 300	2167
CH-ENT-8	0.51	1325	46.947	8.092	4.07	1.34 ± 0.27	3.033	0.970	0.913	600 ± 200	290 ± 80	1083
CH-ENT-9	1.07	1287	46.946	8.092	8.80	3.53 ± 0.28	2.983	0.977	0.915	210 ± 50	230 ± 50	3095
Ent3-1	3.32	1076	46.9561	8.0621	-	1.94 ± 0.11	2.434	0.979	0.954	340 ± 70	1100 ± 200	1912
Ent4-1	54.6	1323	46.9367	8.1049	-	2.43 ± 0.12	3.007	0.965	0.948	320 ± 70	17000 ± 4000	2031
E-5	26.53	1482	46.9235	8.1157	-	3.11 ± 0.17	3.357	0.956	0.937	270 ± 60	7000 ± 1000	2407
E-7a	63.56	1274	46.9411	8.1	-	2.46 ± 0.13	2.922	0.967	0.951	310 ± 60	20000 ± 4000	2097
E-8	8.05	1547	46.9073	8.1074	-	4.60 ± 0.24	3.635	0.959	0.933	200 ± 40	1600 ± 300	3250
E-9	7.83	1537	46.9159	8.0881	-	5.28 ± 0.26	3.369	0.967	0.933	160 ± 30	1300 ± 300	4063
E-10	3.13	1445	46.9417	8.1527	-	4.70 ± 0.21	3.326	0.975	0.935	180 ± 40	600 ± 100	3611
E-11	16.01	1231	46.9393	8.0814	-	2.27 ± 0.13	2.871	0.969	0.949	330 ± 70	5000 ± 1000	1970
E-12	11.71	1280	46.934	8.0763	-	3.53 ± 0.25	2.989	0.964	0.946	220 ± 50	2500 ± 500	2955
E-13	16.64	1534	46.9125	8.0988	-	5.22 ± 0.24	3.511	0.960	0.934	170 ± 30	2800 ± 600	3824
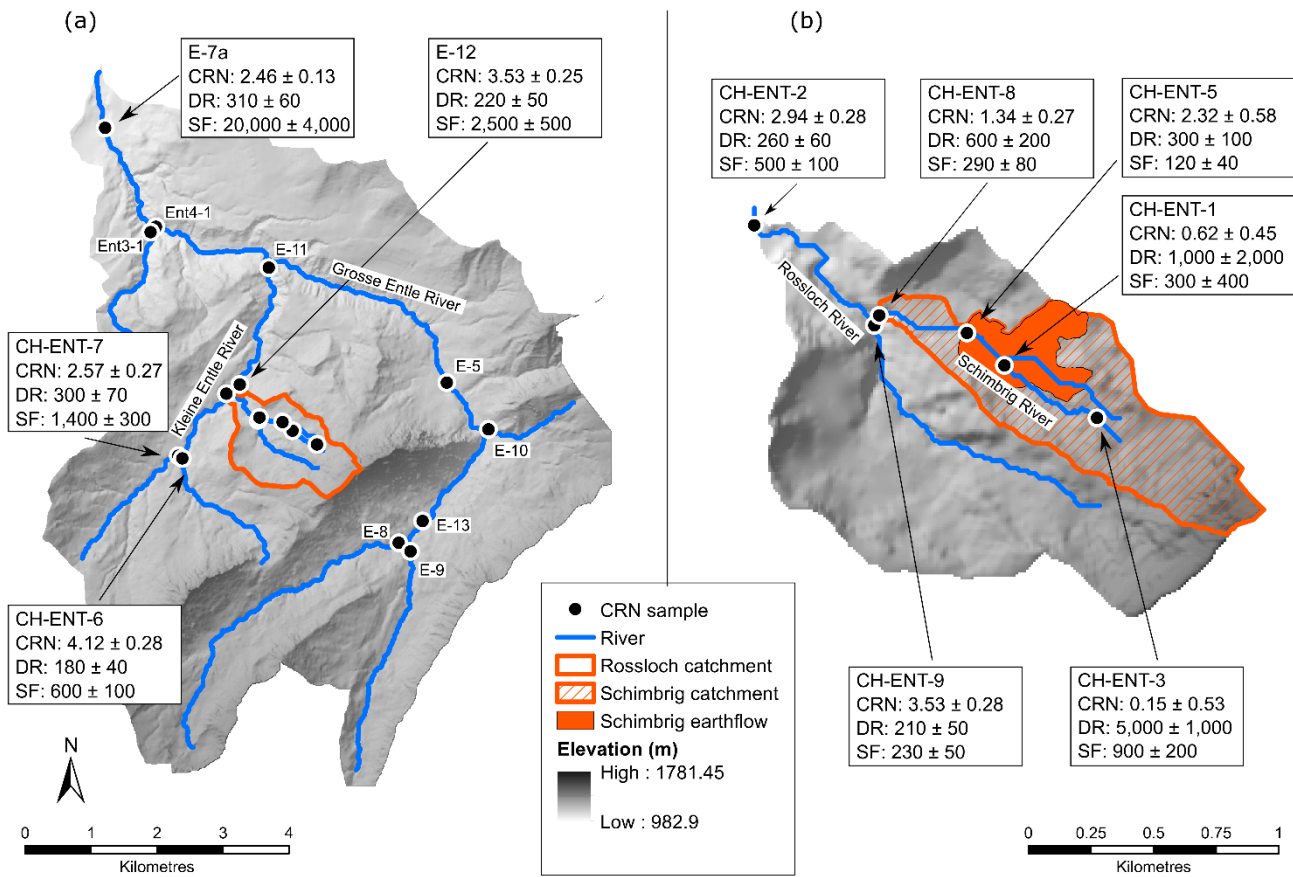
Figure 4: Location of CRN samples in the Entle catchment. CRN concentrations (CRN; ×10³ at g⁻¹), denudation rates (DR; mm kyr⁻¹) and sediment fluxes (SF; m³ yr⁻¹) values displayed are discussed in the text. Other values are available in Table 3. (a) Entle river and (b) Rossloch river catchments. The Schimbrig catchment is depicted by the hatched polygon within the Rossloch catchment in panel (b).

When analysing the ^{10}Be concentrations as a function of distance along the stream, we observe a clear and steady decrease in ^{10}Be concentrations with increasing downstream distance (and catchment area) for the catchments not affected by active mass movements (Figure 4; Figure 5). This decrease in CRN concentrations could, at least in part, results from an increase in erosion rates downstream, as suggested in earlier work by Korup and Schlunegger (2007) and Van den Berg et al. (2012), or from a recycling of buried glacial sediment as the river cuts through 100 m thick unconsolidated glacial deposits in the central part of the catchment (Figure 2).
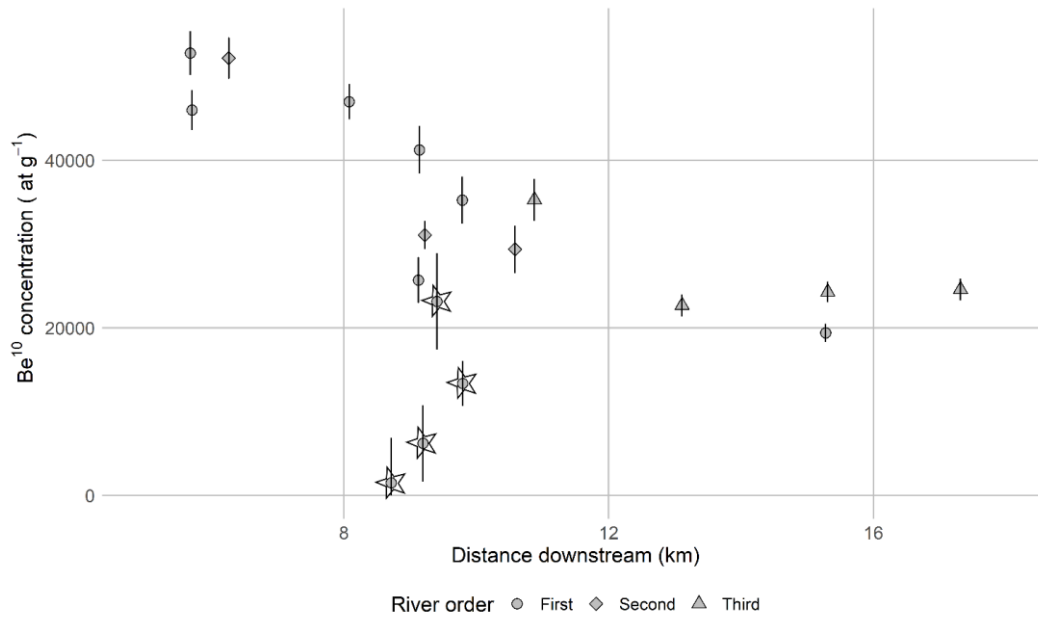
Figure 5: ^{10}Be concentrations (at g^{-1}) along the river network of the Entle catchment. Downstream distance is computed from the river source to the outlet of the Entle catchment. Samples from the earthflow-affected Schimbrig catchment are marked with a *star*.

Figure 5 illustrates the strong contrast in downstream change of ^{10}Be concentrations between the earthflow-affected Schimbrig and nearby catchments. Downslope of the Schimbrig earthflow, the river samples *CH-ENT-1*, *CH-ENT-5* and *CH-ENT-8* have systematically low CRN concentrations that increase downstream. The latter is likely to reflect poor sediment mixing, and long sediment residence time in the alluvial domain. At the confluence with the Rossloch river, the CRN concentration of the earthflow-affected catchment equals 1.34 ± 0.27 at g^{-1} (*CH-ENT-8*), which is at least two times lower than in the neighbouring catchment, i.e. 3.53 ± 0.28 at g^{-1} (*CH-ENT-9*).

5 Discussion

5.1 Sediment fluxes at the millennial scale

Any variation in sediment mixing capacity or delivery from shielded or reworked sediment to the river channel may dilute or increase the concentration in ^{10}Be in river sediments and lead to over- or under-estimation of the catchment-averaged denudation rates and sediment fluxes. Therefore, the geomorphological context of the Entle catchment potentially raises three caveats when using ^{10}Be concentrations measured in fluvial sediments to draw conclusions about the propagation of sediment pulses throughout the landscape. First, the admixture of buried glacial sediments due the incision of the Entle river in a 100 m thick layer of these deposits might lead to dilution of the ^{10}Be signal in the lower reaches. However, in glacial deposits of

nearby sites (Trub river catchment, about 15 km to the West of our study site), Norton et al. (2008) reported ^{10}Be concentrations of glacial deposits reaching $0.76 \pm 0.13 \times 10^4$ at g^{-1} at 8.5 m depth, and $3.58 \pm 0.33 \times 10^4$ at g^{-1} at 1.5 m depth. As these values are about 15% to 50% higher than the catchment-wide CRN concentrations of nearby rivers, the incorporation of buried glacial material in the inner gorge is not the principal cause of the low ^{10}Be concentrations that decrease systematically along the Entle

5   river. Second, along with its small size, the presence of an active earthflow in the Schimbrig catchment might violate the assumption of steady-state denudation and sufficient sediment mixing that are commonly assumed when converting ^{10}Be concentrations of river sediment into catchment-averaged ^{10}Be-derived denudation rates (e.g. Savi et al., 2014; Tofelde et al., 2018). We acknowledge that the dilution of ^{10}Be concentrations in river sediment due to stochastic inputs from landslides might lead to an overestimation of CRN-derived denudation rates (Niemi et al., 2005; Yanites et al., 2009). Therefore, CRN-

10   derived denudation rates and subsequent sediment fluxes presented hereunder will be taken as first order or maximum estimates of the actual values (Puchol et al., 2014). Third, given that sediment production and delivery to the river network is typically stochastic in alpine environments, the ^{10}Be concentrations in river sediment might be highly variable in space and time as shown by Dingle et al., (2018) and West et al., (2014). Figure 5 illustrates the systematic variation in ^{10}Be concentrations in the Entle river basin, and the strong coherence between our dataset, and previously published data by Norton et al (2008) and

15   Van den Berg et al. (2010). As such, the effect of the stochastic input of earthflow-derived sediment is likely to be buffered at the scale of the Schimbrig and Rossloch catchments.

Ignoring samples from the earthflow-affected catchment, the long-term denudation rates correlate positively with downstream distance (Table 3; Figure 4; Figure 6), with values ranging from 160 ± 30 mm kyr^{-1} (*E-9*) to 340 ± 70 mm kyr^{-1} (*Ent3-1*). Characterised by a low variability, these values are akin to ^{10}Be-derived denudation rates measured in similar alpine tectonic

20   settings (e.g. Norton et al., 2008). The increase in denudation rates with downstream distance along the Entle river is triggered by the ongoing relief rejuvenation and incision of the inner gorge after the LGM (Van den Berg et al., 2012). The data also indicate that the river network effectively evacuates sediments supplied to the river channel. Accounting for the drainage area at each sampling location, the long-term sediment fluxes (Table 3; Figure 4; Figure 7) show the same positive correlation with downstream distance. The sediment fluxes range from 600 ± 100 m^3 yr^{-1} in upper first-order catchments (*CH-ENT-6* and *E-*

25   *10*) to $20,000 \pm 4,000$ mm kyr^{-1} at the outlet of the Grosse Entle river (*E-7a*). This two-order-of-magnitude increase in sediment fluxes downstream corroborates the efficient evacuation of sediment in the inner gorge.
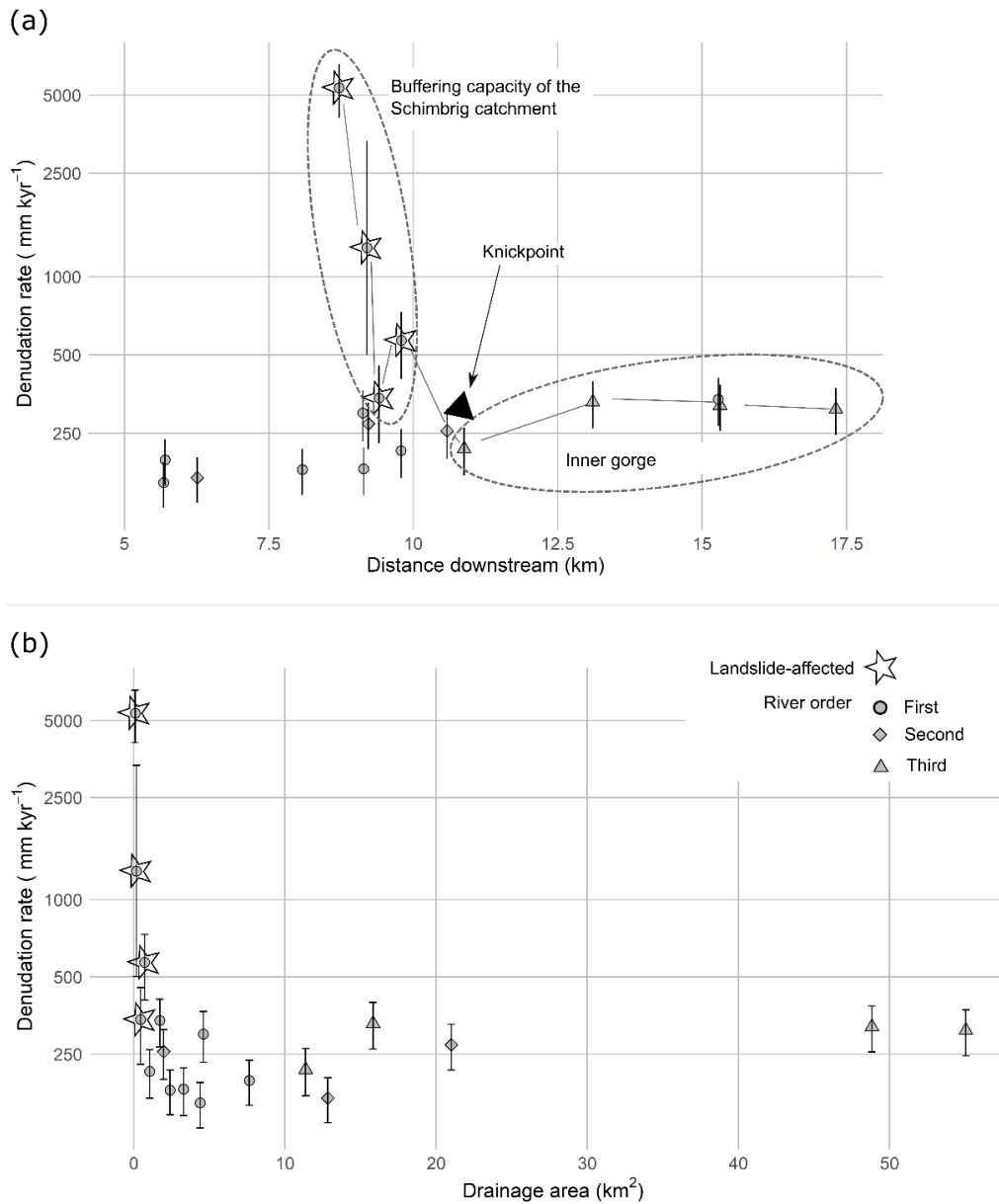
Figure 6: CRN-derived denudation rates (mm kyr⁻¹) in the Entle catchment against (a) downstream distance and (b) drainage area. Downstream distance is computed from the river source to the outlet of the Entle catchment. Samples from the earthflow-affected Schimbrig catchment are marked with a *star*. The grey line connects the points that are hydrologically connected, and part of the same fluvial system (Schimbrig, Rossloch, Kleine Entle and Grosse Entle rivers).

The earthflow-affected catchments show a different pattern that deviates from the overall trend of increasing denudation rates with distance downstream and catchment area. In the first-order Schimbrig catchment, long-term denudation rates correlate negatively with downstream distance (Table 3; Figure 4; Figure 6). The denudation rates of the earthflow-affected first-order catchment are up-to one order of magnitude higher than the rest of the Entle catchment, with values ranging between 300 ± 100 mm kyr^{-1} in the intermediate part (*CH-ENT-5*) and $5,000 \pm 1,000$ mm kyr^{-1} (*CH-ENT-3*) in the upper part of the Schimbrig catchment. The variability in denudation rates along the river is very high, with a one-order of magnitude difference between minimum and maximum values, and spatially highly variable. For example, the denudation rate in *CH-ENT-5* is lower than the sites directly up- and down-stream of this sampling location, reflecting the stochastic character of the sediment delivery from the earthflow. The decrease in denudation rates with catchment area suggests that material initially displaced by the earthflow is not directly evacuated to the river network but remains on the slopes, hence accumulating ^{10}Be atoms in the colluvial domain. Given that the catchment area of the first-order earthflow-affected catchments is small, the absolute sediment fluxes are low with values ranging between 120 ± 40 m^3 yr^{-1} and 900 ± 200 m^3 yr^{-1}. These long-term sediment fluxes computed for the Rossloch catchment, i.e. including the Schimbrig area, are one to two orders of magnitude lower than values computed in other parts of the Entle catchment (Figure 4; Figure 7).
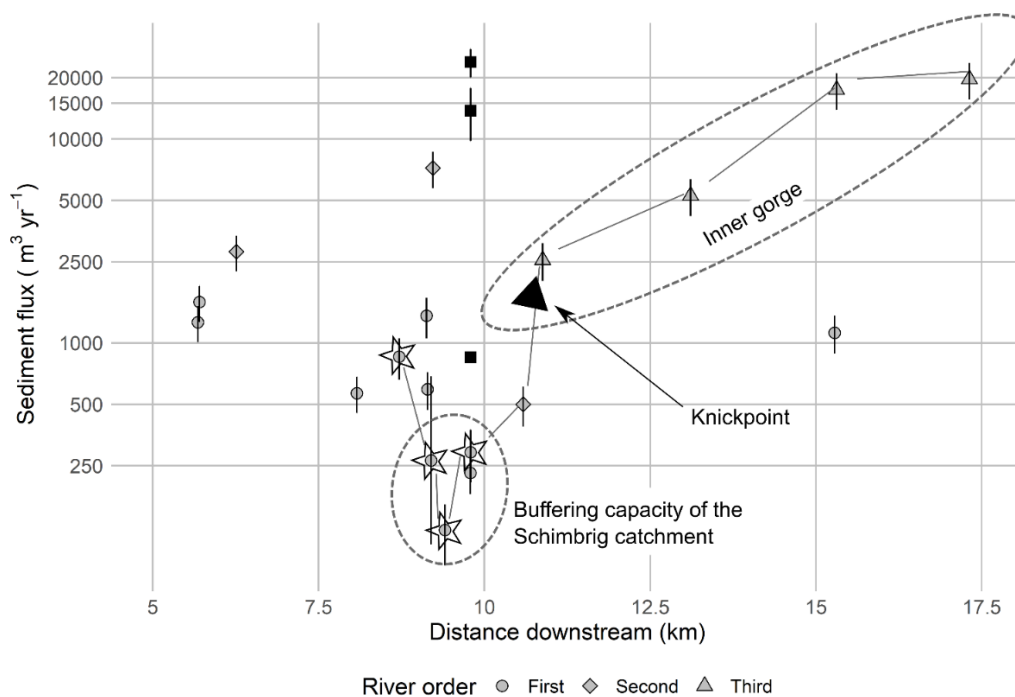
Figure 7: CRN-derived sediment fluxes (m^3 yr^{-1}) along the river network of the Entle catchment. Downstream distance is computed from the river source to the outlet of the Entle catchment. Samples from the earthflow-affected Schimbrig catchment are marked with a *star*. Black square marker represent the sediment flux computed by Schwab et al. (2008) for the period 1962-1998. Grey line presents the downstream sequence of denudation rates along the Schimbrig, Rossloch, Kleine Entle and Grosse Entle rivers.

The impact of landsliding on the long-term sediment dynamics can be evaluated by comparing the denudation rates of the two intersecting catchments at the confluence with the Rossloch river. At the outlet of the Schimbrig catchment, the denudation rate, i.e. 600 ± 200 mm kyr^{-1} (*CH-ENT-8*), is at least two times higher than in the neighbouring catchment, i.e. 210 ± 50 mm kyr^{-1} (*CH-ENT-9*). The difference in denudation rates between the two headwater catchments illustrates that the sediment

5   dynamics of both catchments were probably very different over the last thousands of years as a function of the stochastic input of sediment from landslides (Figure 1). When accounting for their catchment area, the sediment fluxes are very similar though with values of respectively 290 ± 80 m^3 yr^{-1} (*CH-ENT-8*) and 230 ± 50 m^3 yr^{-1} (*CH-ENT-9*).

5.2 Temporal upscaling: The stochastic nature of landsliding

Characterised by a relatively gentle alpine topography, the millennial geomorphic activity of the study area is moderate in
10   intensity. In comparison, the average CRN-derived denudation rate is 270 ± 140 mm kyr^{-1} in similar surrounding areas, i.e. in the Alpine foreland, but increases to 900 ± 300 mm kyr^{-1} in the high crystalline Alps (Wittmann et al., 2007). Dendrogeomorphological data confirmed that the Entle river catchment was affected by an active earthflow at least over the past 150 years (Lopez-Saez et al., 2017; Savi et al., 2013). Given the extent of its active part, i.e. ca. 0.5 km^2, the Schimbrig earthflow is a larger-than-average landslide (Stark and Hovius, 2001). Therefore, according to the magnitude-frequency
15   distribution of landslides (e.g. Hovius et al., 1997), this type of phenomena is generally relatively infrequent, i.e. between 10^{-2} and 10^{-3} events km^{-2} yr^{-1}. The mean annual horizontal displacements (Figure 1a) that we measured within the earthflow, i.e. ca. 6.30 m yr^{-1} for the period 2014-2015, are relatively high in comparison with decimetric displacements reported in the Western Slovakian Carpathians (Prokešová et al., 2014), submetric (< 2 m yr^{-1}) displacementrs reported for the Eel earthflow in California (Mackey et al., 2009), and metric to decametric displacements for the Super-Sauze landslide in Southern French
20   Alps (Niethammer et al., 2012). The toe of the earthflow experienced a downslope movement of ca. 55 m between June 2014 and October 2015 (Figure 1b, Clapuyt et al., 2017). Although the important internal reorganisation of the Schimbrig earthflow, its net sediment budget is roughly in equilibrium: sediment transfer from the colluvial to the fluvial domain (Figure 1c) is minimal over the period 2013-2015. The sediment mobilised by the earthflow is buffered in the colluvial domain, due to decoupling of the hillslope-channel system (Figure 1d) over the annual timescale. In contrast to the limited annual sediment
25   flux (period 2013-2015) of the Schimbrig catchment, its decadal sediment flux (period 1962-1998) equals $13,000 \pm 2,000$ m^3 yr^{-1} (Table 2; Figure 7). The decadal sediment flux is two orders of magnitude higher than the sediment fluxes computed at the millennial time scale over the same spatial extent, i.e. 290 ± 80 m^3 yr^{-1} (*CH-ENT-8*). We note here that the potential overestimation of ^{10}Be-derived denudation rates due to the addition of ^{10}Be-poor material from the earthflow (discussed in 5.1) does not affect our interpretation.

30   The sediment fluxes measured over different timescales reveal the episodic character of sediment production, delivery and transport out of first-order alpine catchments, such as the Schimbrig and Rossloch catchments (Figure 1). Landslides such as the Schimbrig earthflow generate sediment (Figure 1a) that is temporarily stored in the colluvial domain (Figure 1b), and

continues to accumulate [10]Be nuclides during storage. During short phases when hillslope and channel systems are coupled, the colluvial deposits are evacuated out of the first-order sediment stores. The discrepancy between decadal and millennial sediment fluxes illustrates that these phases of hillslope-channel geomorphic coupling are short-lived and intermittent, and interrupt long periods of largely uncoupled colluvial and fluvial geomorphic systems (Figure 8). During most of the time, the first-order catchments are transport-limited, and sediment dynamics in the headwaters are uncoupled from the fluvial systems.
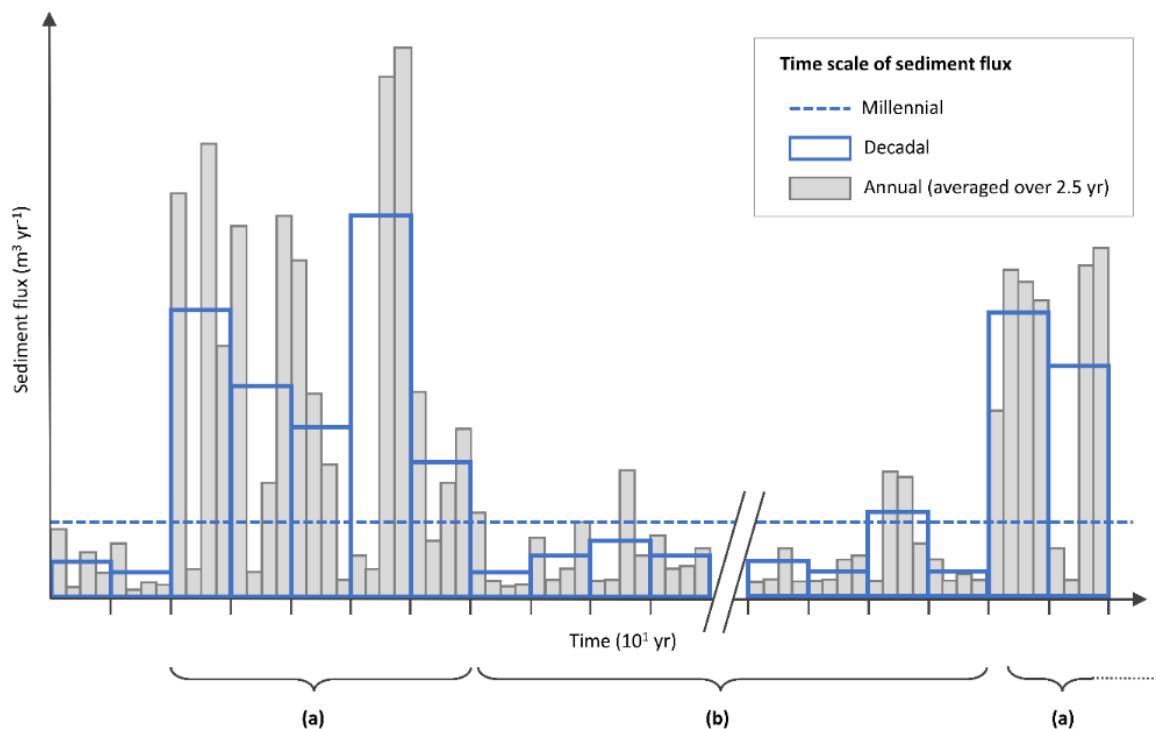
Figure 8: Conceptual representation of the sediment fluxes over different time scales at the outlet of a first-order river catchment. (a) Periods of high hillslope activity due to a landslide sediment pulse, resulting in intermittent hillslope-channel connections and in sediment export to the river network at the annual scale. (b) Periods of low hillslope activity both at the annual and decadal scales, due to poor sediment availability on slopes.

5.3 Spatial upscaling: The importance of landsliding for sediment budgets

Episodic landslides, such as the Schimbrig earthflow, have the potential to mobilise large quantities of sediment at annual or decadal time scale. The average sediment flux at the decadal scale (1962-1998) out of the Schimbrig catchment, i.e. $13,000 \pm 2,000$ m^3 yr^{-1} (Table 2; Figure 7), represents about 65 % of the average sediment flux out of the Entle catchment at the millennial

scale, i.e. 20,000 ± 4,000 m^3 yr^{-1} (*E-7a*; Table 3; Figure 7). This illustrates that landslide-affected catchments can act as principal point sources of sediment, as a sub-catchment covering 1% of the area can provide 65% of the total sediment flux. The higher-order river network, i.e. the Kleine and Grosse Entle rivers, attenuates decadal sediment pulses through the sediment cascade, during which subsequent erosion and deposition occur over centennial time scales. The propagation of the sediment pulses (from e.g. landslides) across the channel network is largely controlled by the hillslope-channel geomorphic coupling, and the transport capacity of the fluvial systems. The latter act as nonlinear filters that smooth out spikes produced by episodic landslide disturbances as also suggested by Jerolmack and Paola (2010). In this sense, we can consider the episodic supply of sediment from landslides during intermittent phases of hillslope-channel coupling as noise that is averaged out when considering sediment fluxes at longer time scales and larger spatial scales. As our data show, one single disturbance (such as an earthflow) has not necessarily an impact on the long-term sediment budget of first-order catchments. Rather, it is the cumulated effect of multiple landslides, which are intermittently connected to the channel network at the decadal scale, along with sediment transport, that may regulate sediment fluxes at the regional spatial scale over the millennial time scale.

6 Conclusion

To better constrain the evacuation of sediment produced by landslides on hillslopes and their propagation in the channel network, we compiled geomorphic assessments at different spatio-temporal scales of the Entle river catchment located in the foothills of the Central Swiss Alps. This 64-km² mountainous river catchment is affected by the Schimbrig earthflow for more than 150 years. We quantified (or took benefit from previous studies of) sediment fluxes over annual, decadal and millennial time scales using respectively UAV-SfM-based 3D topographic reconstructions, classic photogrammetry and in-situ produced [10]Be cosmogenic radionuclides. Our unique spatio-temporal database of sediment fluxes highlights the episodic character of sediment production, delivery and transport out of first-order river catchments i.e. the Schimbrig and Rossloch catchments. A two-order of magnitude discrepancy is observed between annual, decadal and millennial sediment fluxes at the outlet of the Schimbrig catchment. It illustrates that phases of hillslope-channel geomorphic coupling are short-lived and intermittent, and interrupt long periods of largely uncoupled colluvial and fluvial geomorphic systems. During most of the time, the first-order catchments are transport-limited, and sediment dynamics in the headwaters are uncoupled from the fluvial systems.

Landslides such as the Schimbrig earthflow act as point sources of sediment. Although they represent only 1% of the total surface area, they can produce intermittently about 65% of the average regional sediment flux. The impact of a single sediment pulse is strongly attenuated at larger spatial and temporal scales by sediment transport mechanisms. The latter tend to smooth out the spikes in sediment flux delivered by episodic landslide events. Therefore, the accumulation of multiple sediment pulses, which are intermittently delivered to the channel network during phases of hillslope-channel geomorphic coupling, rather have a measurable impact on the regional pattern of sediment fluxes.

Data availability. All datasets and code are available upon request. Please contact the first author for details.

Competing interests. The authors declare that they have no conflict of interest.

Acknowledgments. The Authors would like to thank Jérome Schoonejans for the extended help and the careful supervision of the CRN extraction procedure in the Cosmo Laboratory of the Georges Lemaître Centre for Earth and Climate Research at the Université catholique de Louvain. We extend our thanks to Marco Bravin for the help with sample leaching in the soil lab. We also acknowledge Romain Delunel from Bern Universität for the computation of the snow shielding factors which serves as

10   inputs to derive long-term denudation rates. Efficient and reproducible research is possible thanks to open-source algorithms, such as CAIRN, i.e. the CRN-derived denudation rates calculator, developed by Simon Mudd and his colleagues. Finally, we would like to thank Luca Malatesta and one anonymous reviewer for their constructive comments, which helped us to better structure the manuscript and improve its quality.

6 References

Aalto, R., Dunne, T. and Guyot, J. L.: Geomorphic controls on Andean denudation rates, J. Geol., 114(1), 85–99, doi:10.1086/498101, 2006.

Auer, M.: Regionalisierung von Schneeparametern—Eine Methode zur Darstellung von Schneeparametern imRelief., University of Berne., 2003.

Benda, L. and Dunne, T.: Stochastic forcing of sediment supply to channel networks from landsliding and debris flow, Water Resour. Res., 33(12), 2849–2863, doi:10.1029/97WR02388, 1997.

Bennett, G. L., Molnar, P., McArdell, B. W., Schlunegger, F. and Burlando, P.: Patterns and controls of sediment production, transfer and yield in the Illgraben, Geomorphology, 188, 68–82, doi:10.1016/j.geomorph.2012.11.029, 2013.

Bennett, G. L., Molnar, P., McArdell, B. W. and Burlando, P.: A probabilistic sediment cascade model of sediment transfer in the Illgraben, Water Resour. Res., 50, 1225–1244, doi:doi:10.1002/2013WR013806, 2014.

Berger, C., McArdell, B. W. and Schlunegger, F.: Sediment transfer patterns at the Illgraben catchment, Switzerland: Implications for the time scales of debris flow activities, Geomorphology, 125(3), 421–432, doi:10.1016/j.geomorph.2010.10.019, 2011.

Bracken, L. J., Turnbull, L., Wainwright, J. and Bogaart, P.: Sediment connectivity: A framework for understanding sediment transfer at multiple scales, Earth Surf. Process. Landforms, 40(2), 177–188, doi:10.1002/esp.3635, 2015.

Braucher, R., Merchel, S., Borgomano, J. and Bourlès, D. L.: Production of cosmogenic radionuclides at great depth: A multi element approach, Earth Planet. Sci. Lett., 309(1–2), 1–9, doi:10.1016/j.epsl.2011.06.036, 2011.

Christl, M., Vockenhuber, C., Kubik, P. W., Wacker, L., Lachner, J., Alfimov, V. and Synal, H. A.: The ETH Zurich AMS facilities: Performance parameters and reference materials, Nucl. Instruments Methods Phys. Res. Sect. B Beam Interact. with Mater. Atoms, 294, 29–38, doi:10.1016/j.nimb.2012.03.004, 2013.

Clapuyt, F., Vanacker, V., Schlunegger, F. and Van Oost, K.: Unravelling earth flow dynamics with 3-D time series derived from UAV-SfM models, Earth Surf. Dyn., 5(4), 791–806, doi:10.5194/esurf-5-791-2017, 2017.

Crozier, M. J. and Glade, T.: Frequency and magnitude of landsliding: fundamental research issues, Zeitschrift für Geomorphol. Suppl. Vol., 115, 141–155, doi:10.1127/zfgsuppl/115/1999/141, 1999.

Delong, S. B., Prentice, C. S., Hilley, G. E. and Ebert, Y.: Multitemporal ALSM change detection, sediment delivery, and process mapping at an active earthflow, Earth Surf. Process. Landforms, 37(3), 262–272, doi:10.1002/esp.2234, 2012.

Dingle, E. H., Sinclair, H. D., Attal, M., Rodés, Á. and Singh, V.: Temporal variability in detrital [10]Be concentrations in large Himalayan catchments, Earth Surf. Dyn. Discuss., 1–51, doi:10.5194/esurf-2017-73, 2018.

Fryirs, K.: (Dis)Connectivity in catchment sediment cascades: A fresh look at the sediment delivery problem, Earth Surf. Process. Landforms, 38(1), 30–46, doi:10.1002/esp.3242, 2013.

Fuller, I. C. and Marden, M.: Rapid channel response to variability in sediment supply: Cutting and filling of the Tarndale Fan, Waipaoa catchment, New Zealand, Mar. Geol., 270(1–4), 45–54, doi:10.1016/j.margeo.2009.10.004, 2010.

5   Gong, G.: Physical Properties of Alpine Rocks : A Laboratory Investigation, University of Geneva., 2005.

Gran, K. B. and Czuba, J. A.: Sediment pulse evolution and the role of network structure, Geomorphology, 277, 17–30, doi:10.1016/j.geomorph.2015.12.015, 2017.

Harvey, A. M.: Coupling between hillslopes and channels in upland fluvial systems: implications for landscape sensitivity, illustrated from the Howgill Fells, northwest England, Catena, (42), 225–250, 2001.

10   Heckmann, T. and Schwanghart, W.: Geomorphic coupling and sediment connectivity in an alpine catchment - Exploring sediment cascades using graph theory, Geomorphology, 182, 89–103, doi:10.1016/j.geomorph.2012.10.033, 2013.

Hovius, N., Stark, C. P. and Allen, P. A.: Sediment flux from a mountain belt derived by landslide mapping, Geology, 25, 231–234, doi:10.1130/0091-7613(1997)025<0231, 1997.

James, M. R., Robson, S. and Smith, M. W.: 3-D uncertainty-based topographic change detection with structure-from-motion
15   photogrammetry: Precision maps for ground control and directly georeferenced surveys, Earth Surf. Process. Landforms, 1788(March), 1769–1788, doi:10.1002/esp.4125, 2017.

Jerolmack, D. J. and Paola, C.: Shredding of environmental signals by sediment transport, Geophys. Res. Lett., 37(19), 1–5, doi:10.1029/2010GL044638, 2010.

Jonas, T., Marty, C. and Magnusson, J.: Estimating the snow water equivalent from snow depth measurements in the Swiss
20   Alps, J. Hydrol., 378(1–2), 161–167, doi:10.1016/j.jhydrol.2009.09.021, 2009.

Korup, O. and Schlunegger, F.: Bedrock landsliding, river incision, and transience of geomorphic hillslope-channel coupling: Evidence from inner gorges in the Swiss Alps, J. Geophys. Res. Earth Surf., 112(3), doi:10.1029/2006JF000710, 2007.

Korup, O., Densmore, A. L. and Schlunegger, F.: The role of landslides in mountain range evolution, Geomorphology, 120(1–2), 77–90, doi:10.1016/j.geomorph.2009.09.017, 2010.

25   Lateltin, A., Beer, O., Raetzo, C., Lateltin, O., Raetzo, H. and Caron, C.: Landslides in flysch terranes of Switzerland : causal factors and climate change Landslides in Flysch terranes of Switzerland : Causal factors and climate change, Eclogae Geol. Helv., 90, 401–406, 1997.

Lopez-Saez, J., Morel, P., Corona, C., Bommer-Denns, B., Schlunegger, F., Berger, F. and Stoffel, M.: Tree-ring reconstruction of reactivation phases of the Schimbrig landslide (Swiss Alps), Géomorphologie Reli. Process. Environ., 23(3), 265–276, doi:10.4000/geomorphologie.11825, 2017.

Mackey, B. H., Roering, J. J. and McKean, J. a.: Long-term kinematics and sediment flux of an active earthflow, Eel River, California, Geology, 37(9), 803–806, doi:10.1130/G30136A.1, 2009.

Malamud, B. D., Turcotte, D. L., Guzzetti, F. and Reichenbach, P.: Landslide inventories and their statistical properties, Earth Surf. Process. Landforms, 29(6), 687–711, doi:10.1002/esp.1064, 2004.

Montgomery, D. R. and Brandon, M. T.: Topographic controls on erosion rates in tectonically active mountain ranges, Earth Planet. Sci. Lett., 201(3–4), 481–489, doi:10.1016/S0012-821X(02)00725-2, 2002.

Mudd, S. M., Harel, M. A., Hurst, M. D., Grieve, S. W. D. and Marrero, S. M.: The CAIRN method: Automated, reproducible calculation of catchment-averaged denudation rates from cosmogenic nuclide concentrations, Earth Surf. Dyn., 4(3), 655–674, doi:10.5194/esurf-4-655-2016, 2016.

Niemi, N. a., Oskin, M., Burbank, D. W., Heimsath, A. M. and Gabet, E. J.: Effects of bedrock landslides on cosmogenically determined erosion rates, Earth Planet. Sci. Lett., 237(3–4), 480–498, doi:10.1016/j.epsl.2005.07.009, 2005.

Niethammer, U., James, M. R., Rothmund, S., Travelletti, J. and Joswig, M.: UAV-based remote sensing of the Super-Sauze landslide: Evaluation and results, Eng. Geol., 128, 2–11, doi:10.1016/j.enggeo.2011.03.012, 2012.

Norton, K. P., von Blanckenburg, F., Schlunegger, F., Schwab, M. and Kubik, P. W.: Cosmogenic nuclide-based investigation of spatial erosion and hillslope channel coupling in the transient foreland of the Swiss Alps, Geomorphology, 95(3–4), 474–486, doi:10.1016/j.geomorph.2007.07.013, 2008.

Prokešová, R., Kardoš, M., Táborík, P., Medveďová, A., Stacke, V. and Chudý, F.: Kinematic behaviour of a large earthflow defined by surface displacement monitoring, DEM differencing, and ERT imaging, Geomorphology, 224, 86–101, doi:10.1016/j.geomorph.2014.06.029, 2014.

Puchol, N., Lavé, J., Lupker, M., Blard, P.-H., Gallo, F., France-Lanord, C. and Team, A.: Grain-size dependent concentration of cosmogenic ^{10}Be and erosion dynamics in a landslide-dominated Himalayan watershed, Geomorphology, 224, 55–68, doi:10.1016/j.geomorph.2014.06.019, 2014.

Savi, S., Schneuwly-Bollschweiler, M., Bommer-Denns, B., Stoffel, M. and Schlunegger, F.: Geomorphic coupling between hillslopes and channels in the Swiss Alps, Earth Surf. Process. Landforms, 38(9), 959–969, doi:10.1002/esp.3342, 2013.

Savi, S., Norton, K., Picotti, V., Brardinoni, F., Akçar, N., Kubik, P. W., Delunel, R. and Schlunegger, F.: Effects of sediment mixing on [10]Be concentrations in the Zielbach catchment, central-eastern Italian Alps, Quat. Geochronol., 19, 148–162, doi:10.1016/j.quageo.2013.01.006, 2014.

Schlunegger, F., Jost, J., Grünig, A. and Trüssel, M.: Erläuterungen, Geologischer Atlas der Schweiz, Kartenblatt 1169
5 Schüpfheim 1:25'000, Bundesamt für Landestopographie swisstopo, 107pp, 2016a.

Schlunegger, F., Anspach, O., Bieri, B., Böning, P., Kaufmann, Y., Lahl, K., Lonschinski, M., Mollet, H., Sachse, D., Schubert, C., Stöckli, G. and Zander, I.: Geologische Karte der Schweiz, Kartenblatt 1169 Schüpfheim 1:25'000, Bundesamt für Landestopographie swisstopo, 2016b.

Schwab, M., Rieke-Zapp, D., Schneider, H., Liniger, M. and Schlunegger, F.: Landsliding and sediment flux in the Central
10 Swiss Alps: A photogrammetric study of the Schimbrig landslide, Entlebuch, Geomorphology, 97(3–4), 392–406, doi:10.1016/j.geomorph.2007.08.019, 2008.

Stark, C. P. and Hovius, N.: The characterization of landslide size distribution, Geophys. Res. Lett., 28(6), 1091–1094, 2001.

Sutherland, D. G., Ball, M. H., Hilton, S. J. and Lisle, T. E.: Evolution of a landslide-induced sediment wave in the Navarro River, California, Bull. Geol. Soc. Am., 114(8), 1036–1048, doi:10.1130/0016-7606(2002)114<1036:EOALIS>2.0.CO;2,
15 2002.

Tofelde, S., Duesing, W., Schildgen, T. F., Wickert, A. D., Wittmann, H., Alonso, R. N. and Strecker, M.: Effects of deep-seated versus shallow hillslope processes on cosmogenic [10]Be concentrations in fluvial sand and gravel, Earth Surf. Process. Landforms, doi:10.1002/esp.4471, 2018.

Vanacker, V., Vanderschaeghe, M., Govers, G., Willems, E., Poesen, J., Deckers, J. and De Bievre, B.: Linking hydrological,
20 infinite slope stability and land-use change models through GIS for assessing the impact of deforestation on slope stability in high Andean watersheds, Geomorphology, 52(3–4), 299–315, doi:10.1016/S0169-555X(02)00263-5, 2003.

Vanacker, V., von Blanckenburg, F., Hewawasam, T. and Kubik, P. W.: Constraining landscape development of the Sri Lankan escarpment with cosmogenic nuclides in river sediment, Earth Planet. Sci. Lett., 253(3–4), 402–414, doi:10.1016/j.epsl.2006.11.003, 2007.

25 Van den Berg, F., Schlunegger, F., Akçar, N. and Kubik, P.: [10]Be-derived assessment of accelerated erosion in a glacially conditioned inner gorge, Entlebuch, Central Alps of Switzerland, Earth Surf. Process. Landforms, 37(11), 1176–1188, doi:10.1002/esp.3237, 2012.

Walling, D. E.: The sediment delivery problem, J. Hydrol., 65(1–3), 209–237, doi:10.1016/0022-1694(83)90217-2, 1983.

Wang, W., Godard, V., Liu-Zeng, J., Scherler, D., Xu, C., Zhang, J., Xie, K., Bellier, O., Ansberque, C., de Sigoyer, J. and Team, A.: Perturbation of fluvial sediment fluxes following the 2008 Wenchuan earthquake, Earth Surf. Process. Landforms, 42(15), 2611–2622, doi:10.1002/esp.4210, 2017.

West, A. J., Hetzel, R., Li, G., Jin, Z., Zhang, F., Hilton, R. G. and Densmore, A. L.: Dilution of [10]Be in detrital quartz by earthquake-induced landslides: Implications for determining denudation rates and potential to provide insights into landslide sediment dynamics, Earth Planet. Sci. Lett., 396, 143–153, doi:10.1016/j.epsl.2014.03.058, 2014.

Wheaton, J. M., Brasington, J., Darby, S. E. and Sear, D. a.: Accounting for uncertainty in DEMs from repeat topographic surveys: improved sediment budgets, Earth Surf. Process. Landforms, 35, 136–156, doi:10.1002/esp.1886, 2010.

Whipple, K. X. and Tucker, G. E.: Dynamics of the stream-power river incision model: Implications for height limits of mountain ranges, landscape response timescales, and research needs, J. Geophys. Res., 104(B8), 17661–17674, doi:10.1029/1999JB900120, 1999.

Wittmann, H., von Blanckenburg, F., Kruesmann, T., Norton, K. P. and Kubik, P. W.: Relation between rock uplift and denudation from cosmogenic nuclides in river sediment in the Central Alps of Switzerland, J. Geophys. Res. Earth Surf., 112(4), 1–20, doi:10.1029/2006JF000729, 2007.

Yanites, B. J., Tucker, G. E. and Anderson, R. S.: Numerical and analytical models of cosmogenic radionuclide dynamics in landslide-dominated drainage basins, J. Geophys. Res. Earth Surf., 114(1), doi:10.1029/2008JF001088, 2009.